Supplementary information

Lithium-rich sulfide $Li_2Ti_{1-x}Si_xS_3$ cathode materials optimized through Si-doping for high-capacity all-solid-state lithium-ion batteries

*Yaqi Hu [a], Zongliang Zhang [b], Siliang Liu [a], Fangbo He [c], Yang Liu [c], Zhi Zhuang [c], Fangyang Liu [a]**

[a] School of Metallurgy and Environment, Central South University, Changsha, Hunan, 410083, P. R. China

[b] Hunan Provincial Key Laboratory of Nonferrous Value-added Metallurgy, Changsha, Hunan, 410083, P. R. China

[c] Hunan Energy Frontiers New Materials Technology Co., LTD

***Corresponding author**

liufangyang@csu.edu.cn

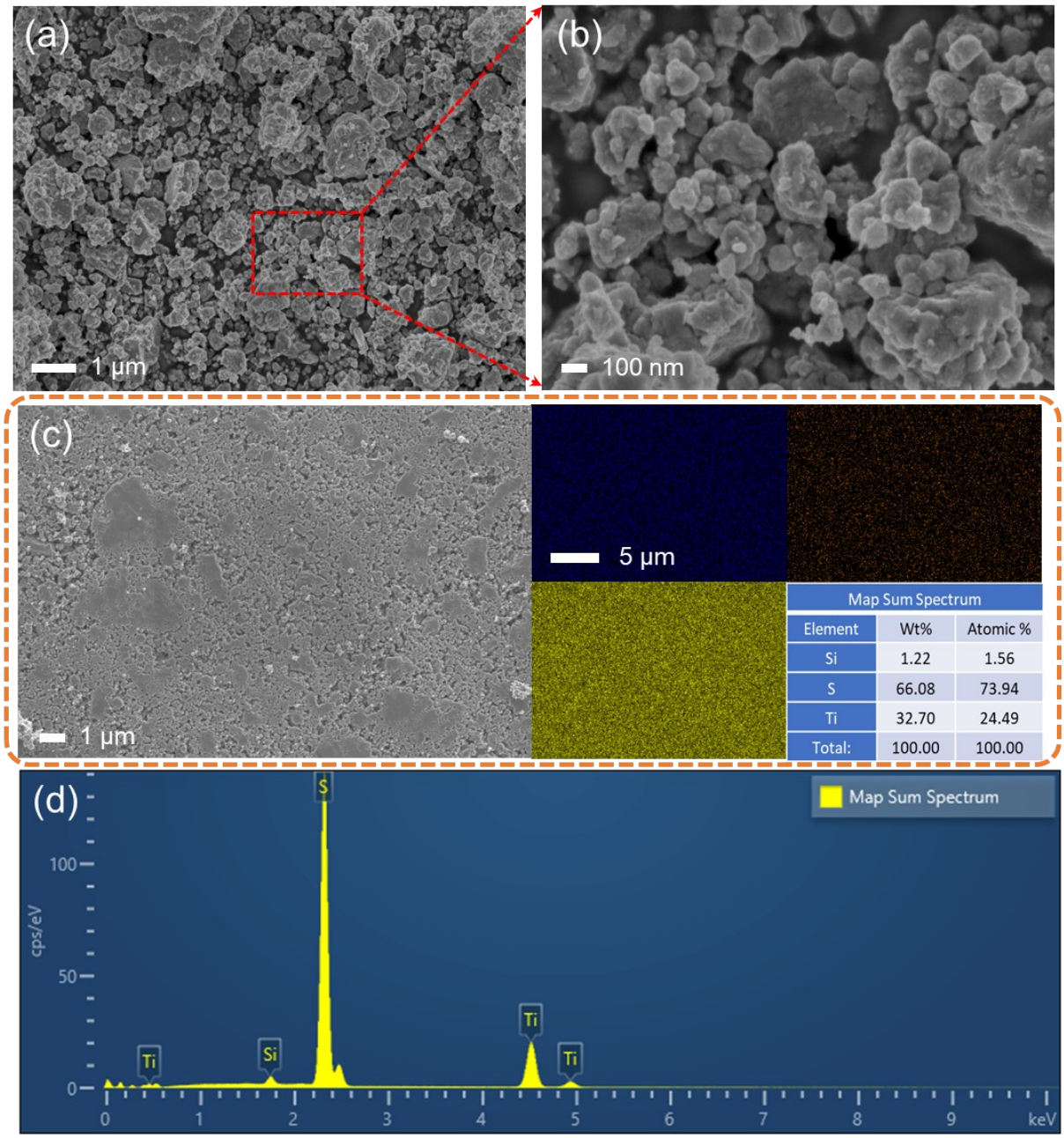

Figure S1 (a) (b) SEM images of R-$Li_2Ti_{1-x}Si_xS_3$. (c) SEM-EDS images and (d) Map Sum Spectrum of the surface on the compacted R-$Li_2Ti_{1-x}Si_xS_3$ pellet.

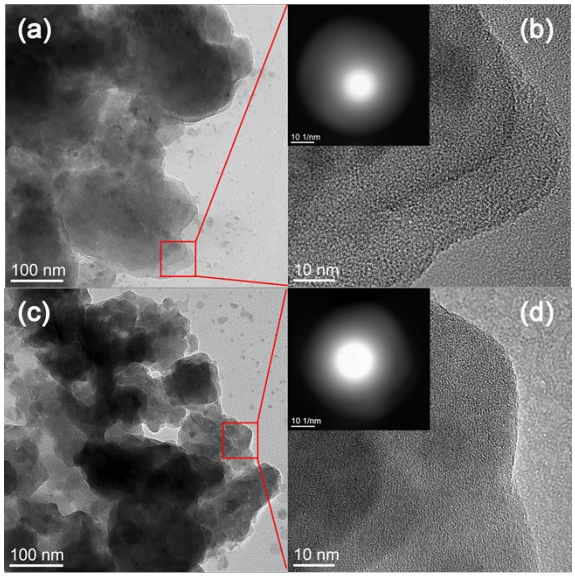

Figure S2 TEM and SAED images of (a) (b) R-Pristine and (c) (b) R-6%Si.

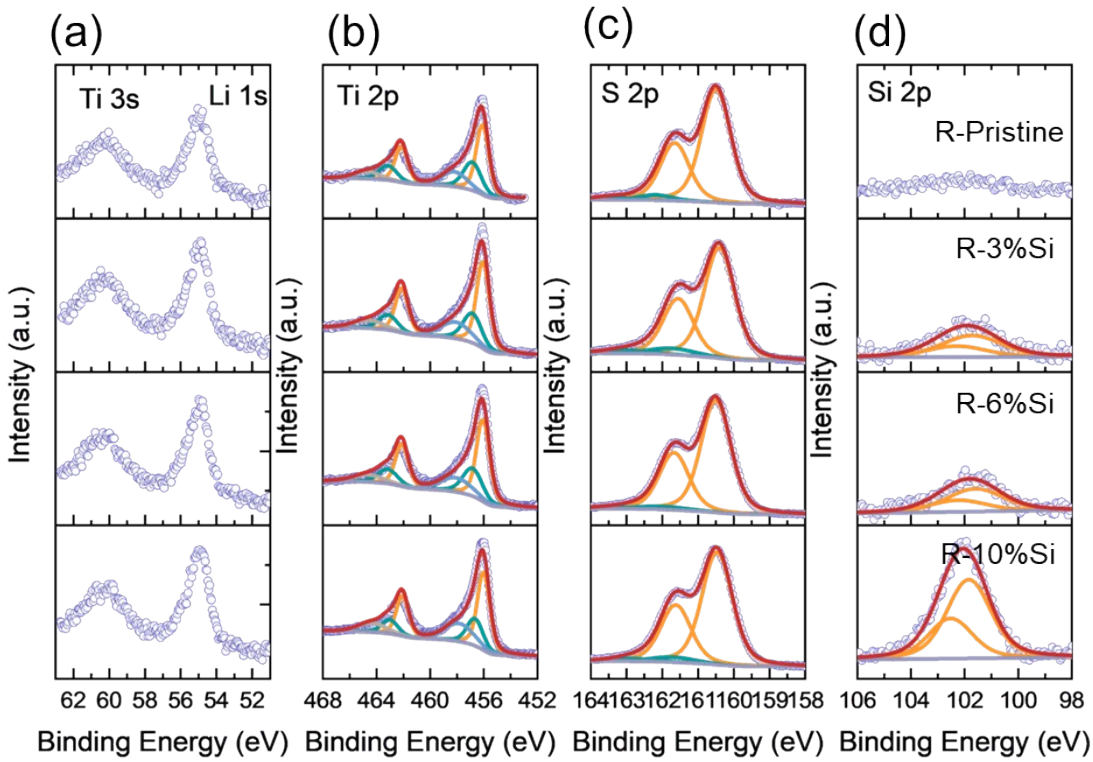

Figure S3 (a) Li 1s, (b) Ti 2p, (c) S 2p, and (d) Si 2p XPS spectra of the surface region on R-$Li_2Ti_{1-x}Si_xS_3$.

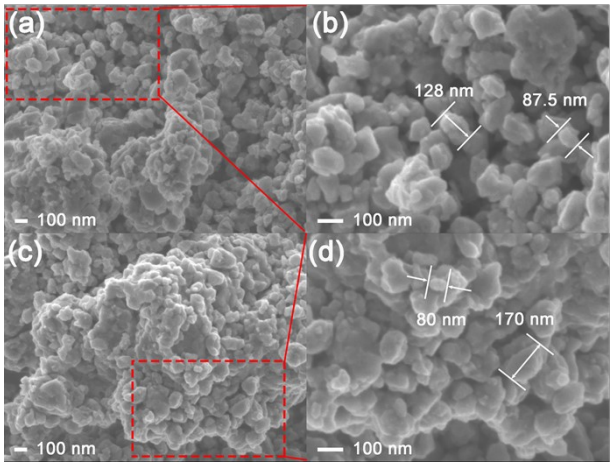

Figure S4 SEM images of (a) (b) L-Pristine and (c) (d) L-10%Si.

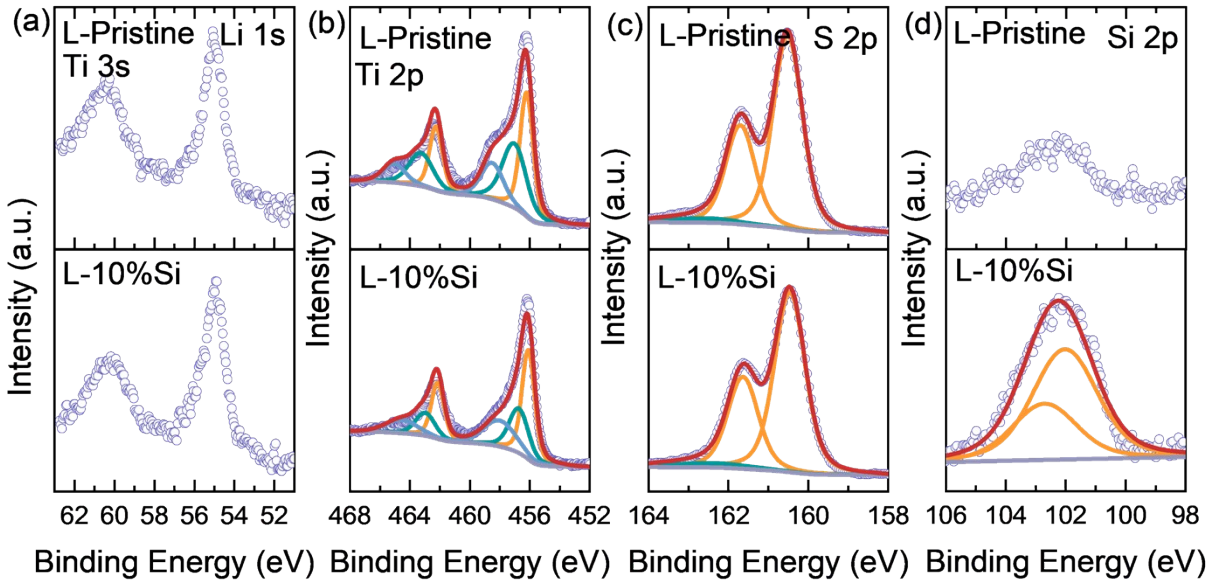

Figure S5 (a) Li 1s, (b) Ti 2p, (c) S 2p, and (d) Si 2p XPS spectra of L-Prisine and L-10%Si.

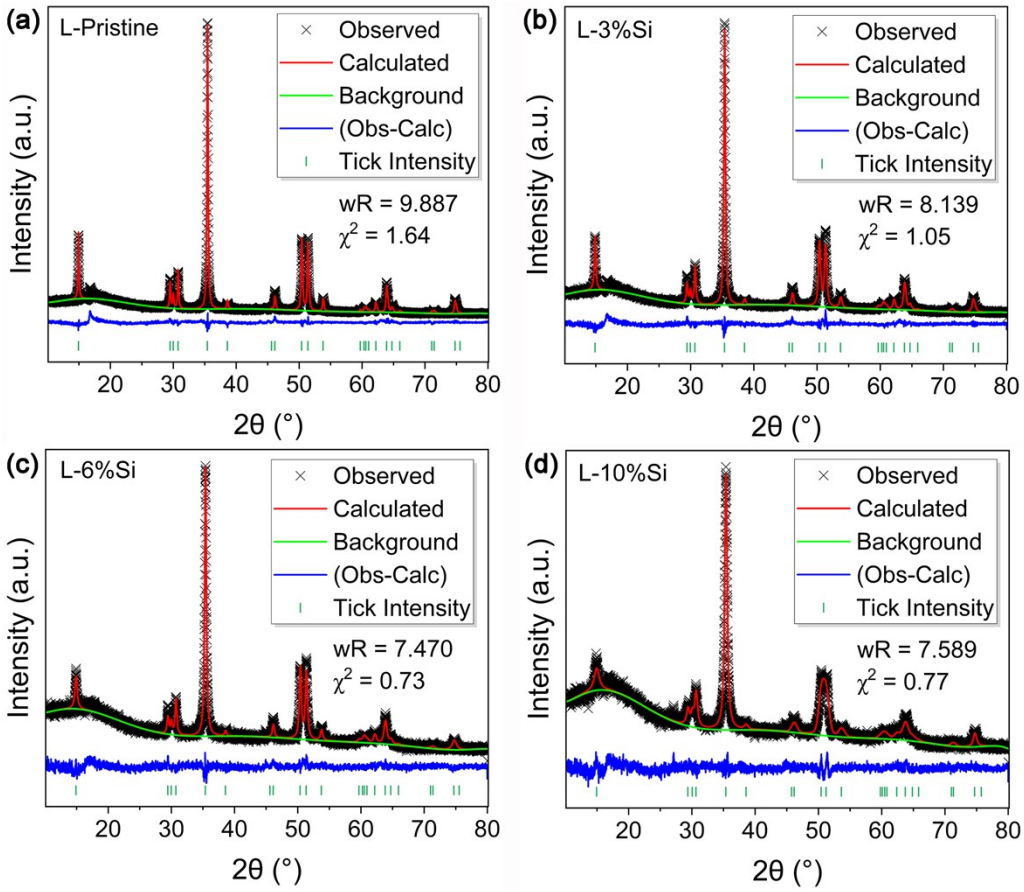

Figure S6 Refined XRD patterns of (f) L-Pristine, (g) L-3%Si, (h) L-6%Si and (i) L-10%Si.

Table S1 Refined structural parameters of L-Pristine.

Atom	x	y	z	Wyckoff	Frac	Uiso
Li(0)	0	0	0	3a	0.9009	0.17774
Ti(1)	0	0	0	3a	0.0991	0.17774
Li(2)	0	0	0.5	3b	0.4291	0.00205
Ti(3)	0	0	0.5	3b	0.5709	0.00205
S(4)	0	0	0.24726	6c	1.0000	0.02809
a= b= 3.55956, c= 17.92400. wR= 9.887, χ^2= 1.64						

Table S2 Refined structural parameters of L-3%Si.

Atom	x	y	z	Wyckoff	Occu.	Uiso
Li(0)	0	0	0	3a	0.8940	0.13509
Ti(1)	0	0	0	3a	0.0991	0.13509
Li(2)	0	0	0.5	3b	0.4360	0.00241
Ti(3)	0	0	0.5	3b	0.5441	0.00241
S(4)	0	0	0.24646	6c	1.0000	0.01795
Si(5)	0	0	0	3a	0.0069	0.13509
Si(6)	0	0	0.5	3b	0.0199	0.00241
a= b= 3.56101, c= 17.91790. wR= 8.139, χ^2= 1.05						

Table S3 Refined structural parameters of L-6%Si.

Atom	x	y	z	Wyckoff	Occu.	Uiso
Li(0)	0	0	0	3a	0.8855	0.12771
Ti(1)	0	0	0	3a	0.1027	0.12771
Li(2)	0	0	0.5	3b	0.4445	0.00307
Ti(3)	0	0	0.5	3b	0.5271	0.00307
S(4)	0	0	0.24641	6c	1.0000	0.01514
Si(5)	0	0	0	3a	0.0118	0.12771
Si(6)	0	0	0.5	3b	0.0284	0.00307
a= b= 3.56320, c= 17.92628. wR= 7.47, χ^2= 0.73						

Table S4 Refined structural parameters of L-10%Si.

Atom	x	y	z	Wyckoff	Occu.	Uiso
Li(0)	0	0	0	3a	0.8603	0.22559
Ti(1)	0	0	0	3a	0.0890	0.22559
Li(2)	0	0	0.5	3b	0.4697	0.00352
Ti(3)	0	0	0.5	3b	0.5073	0.00352
S(4)	0	0	0.24618	6c	1.0000	0.03031
Si(5)	0	0	0	3a	0.0507	0.22559
Si(6)	0	0	0.5	3b	0.0230	0.00352
a= b= 3.56999, c= 17.86797. wR= 7.589, χ^2= 0.77						

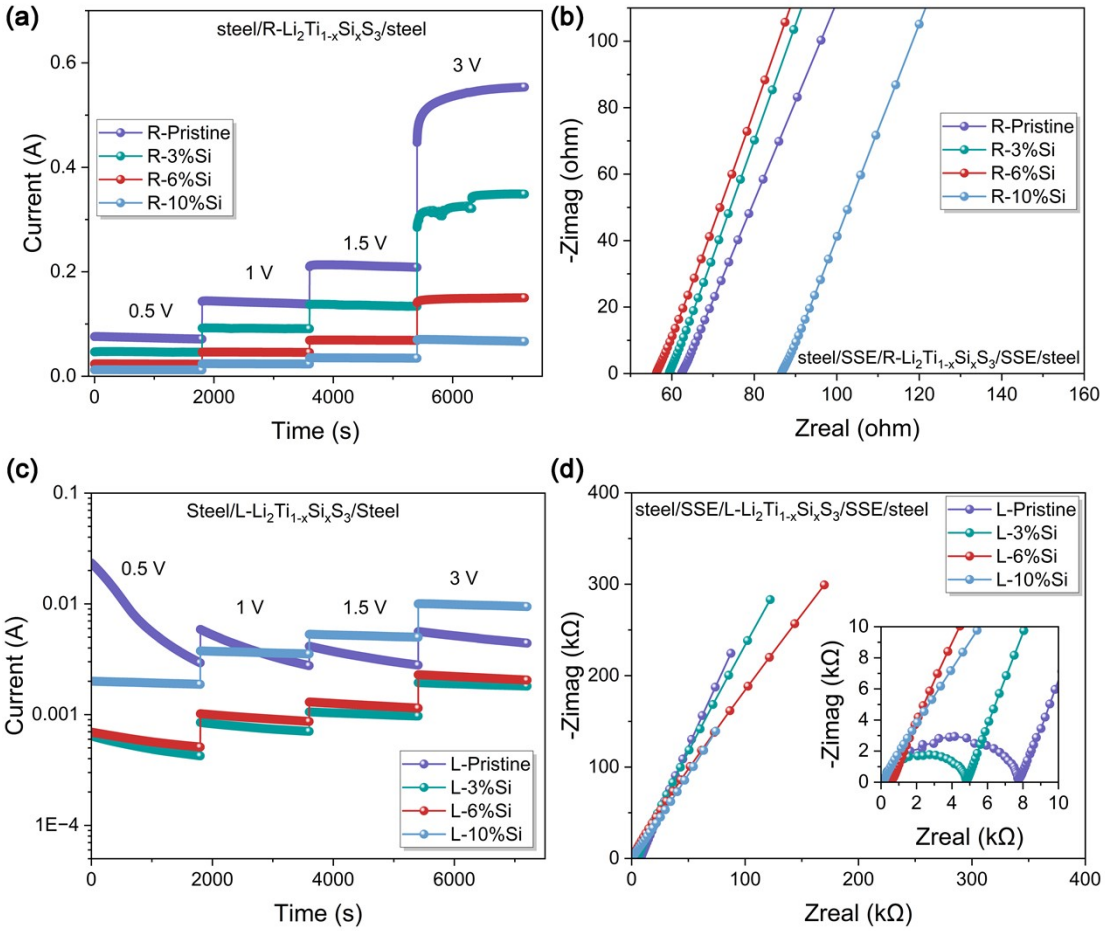

Figure S7 DC polarization plots of (a) R-$Li_2Ti_{1-x}Si_xS_3$ and (c) L-$Li_2Ti_{1-x}Si_xS_3$ under different bias voltages. AC impedance plots of (b) R-$Li_2Ti_{1-x}Si_xS_3$ and (d) L-$Li_2Ti_{1-x}Si_xS_3$.

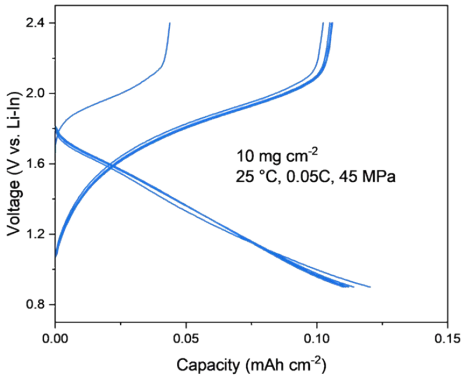

Figure S8 Charge/discharge curves of R-$Li_2Ti_{1-x}Si_xS_3$ at 0.05C and 25 °C without any conductive additives.

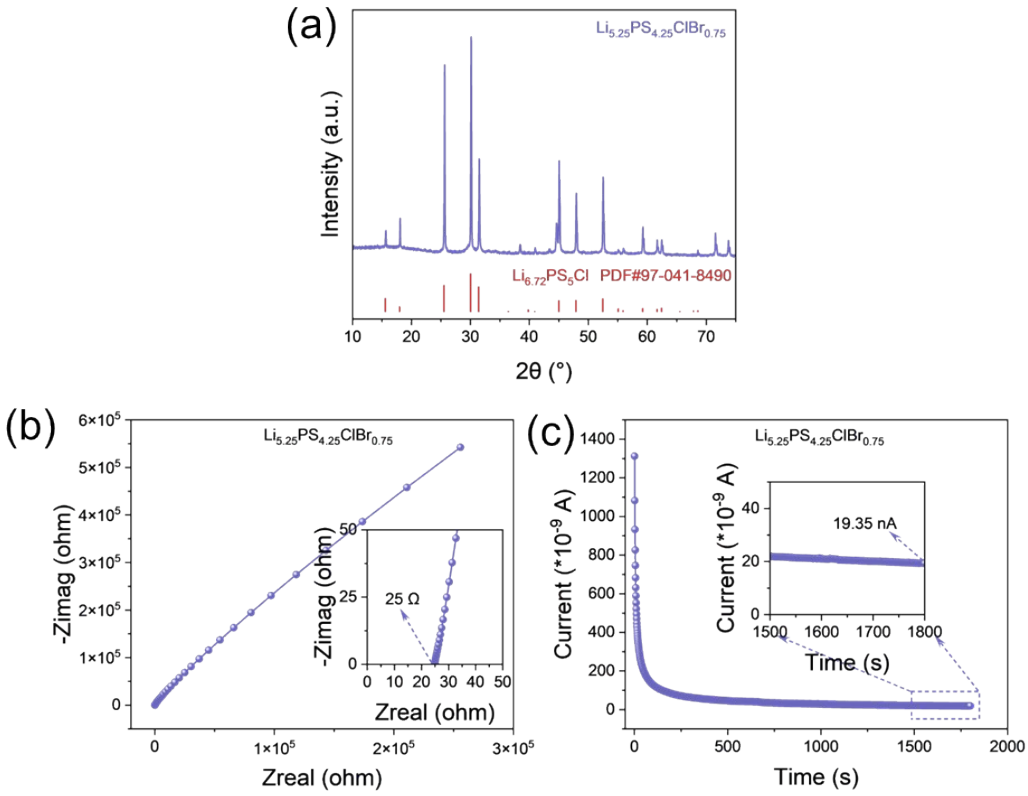

Figure S9 (a) XRD pattern, (b) AC impedance plot, and (c) DC polarization plot of $Li_{5.25}PS_{4.25}ClBr_{0.75}$.

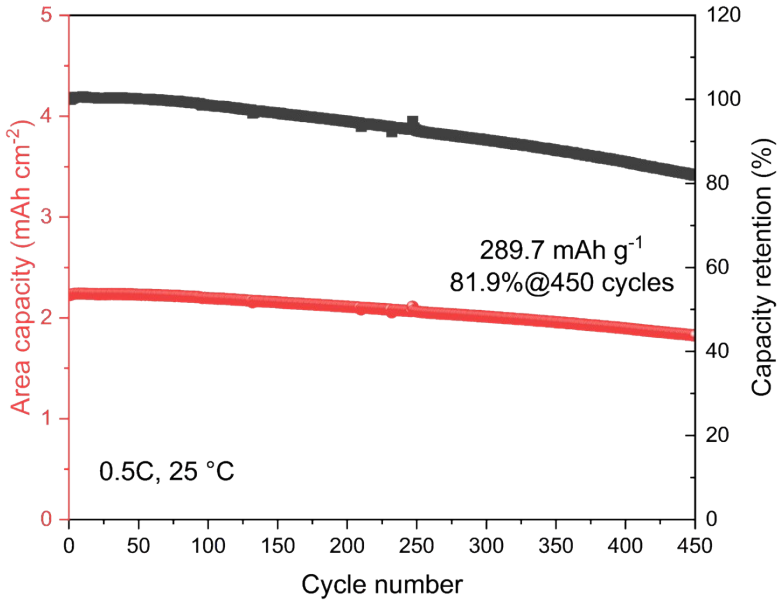

Figure S10 Cycling performance of R-6%Si at 0.5C and 25 °C.

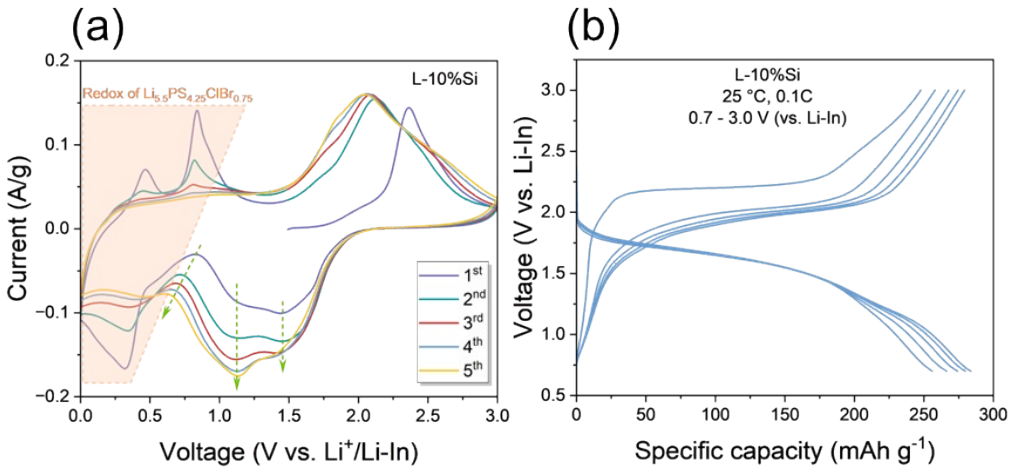

Figure S11 The CV curves of L-10%Si at 0 - 3.0 V (vs. Li-In). (b) The charge-discharge profiles at the first five cycles with the discharge potential extending to 0.7 V (vs. Li-In).

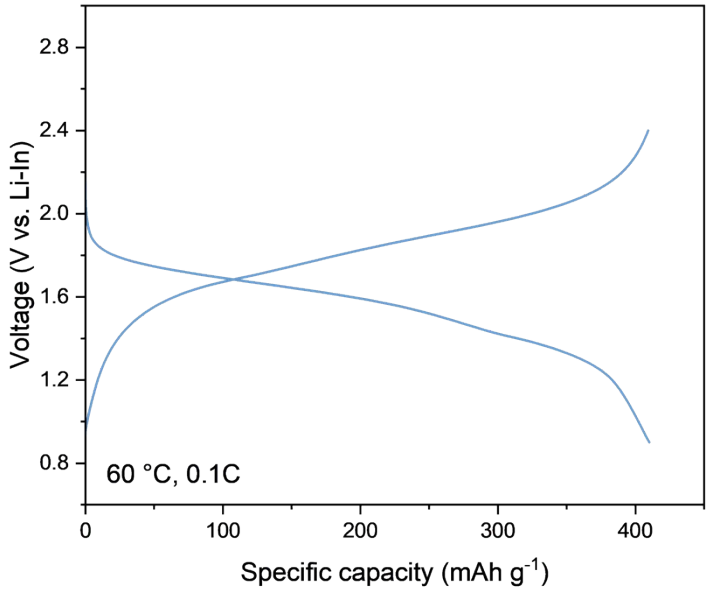

Figure S12 The charge-discharge curve of the cell based on the high-loading cathode film. at 60°C, achieving a discharge capacity of 410.19 mAh g^{-1}.

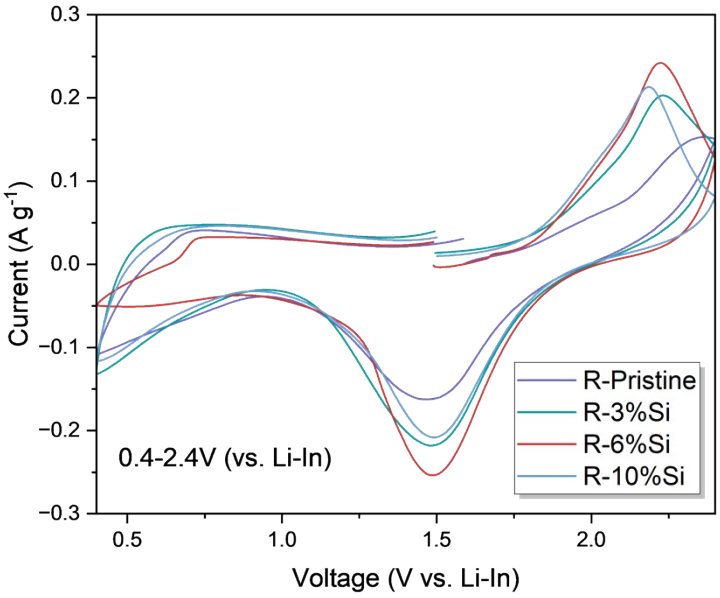

Figure S13 The CV curves of the R-$Li_2Ti_{1-x}Si_xS_3$ cathodes.

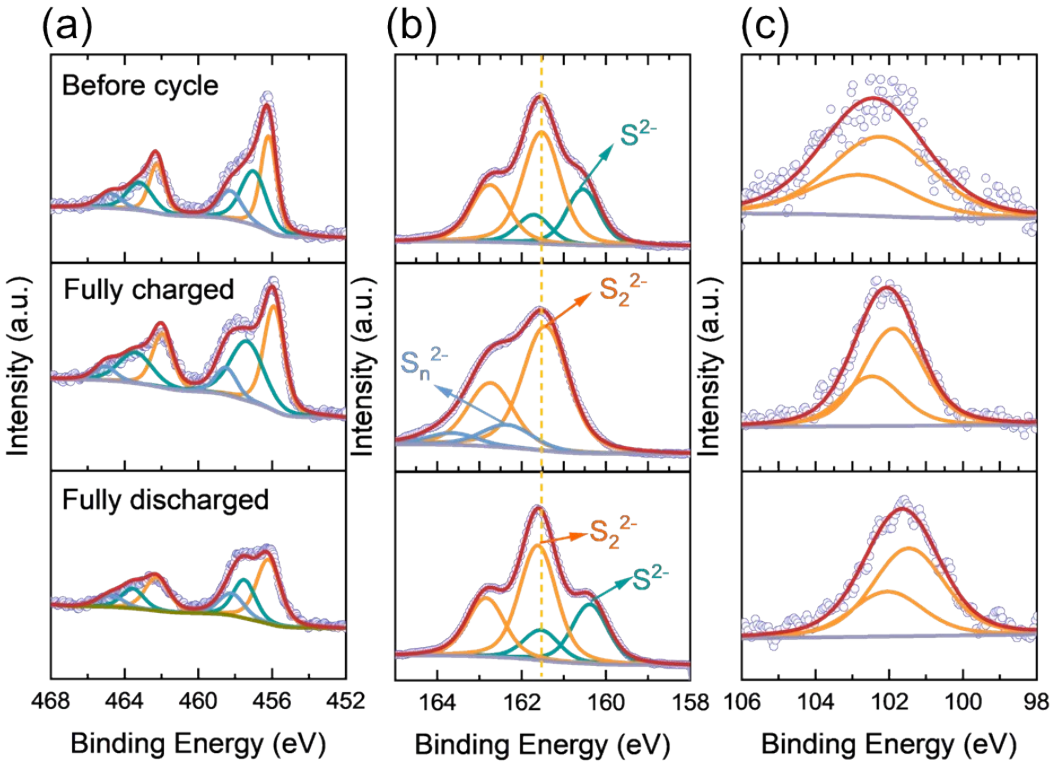

Figure S14 (a) Ti 2p, (b) S 2p, and (c) Si 2p XPS spectra of the R-6%Si cathode in different charge of state at the first cycle.

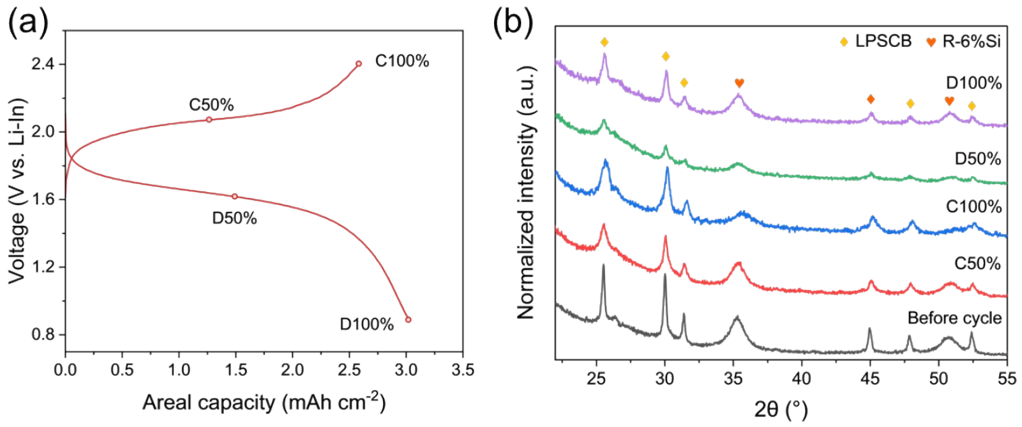

Figure S15 (a) Charge-discharge curve of R-6%Si. (b) Normalized XRD patterns of the R-6%Si cathode in different charge of state at the first cycle.

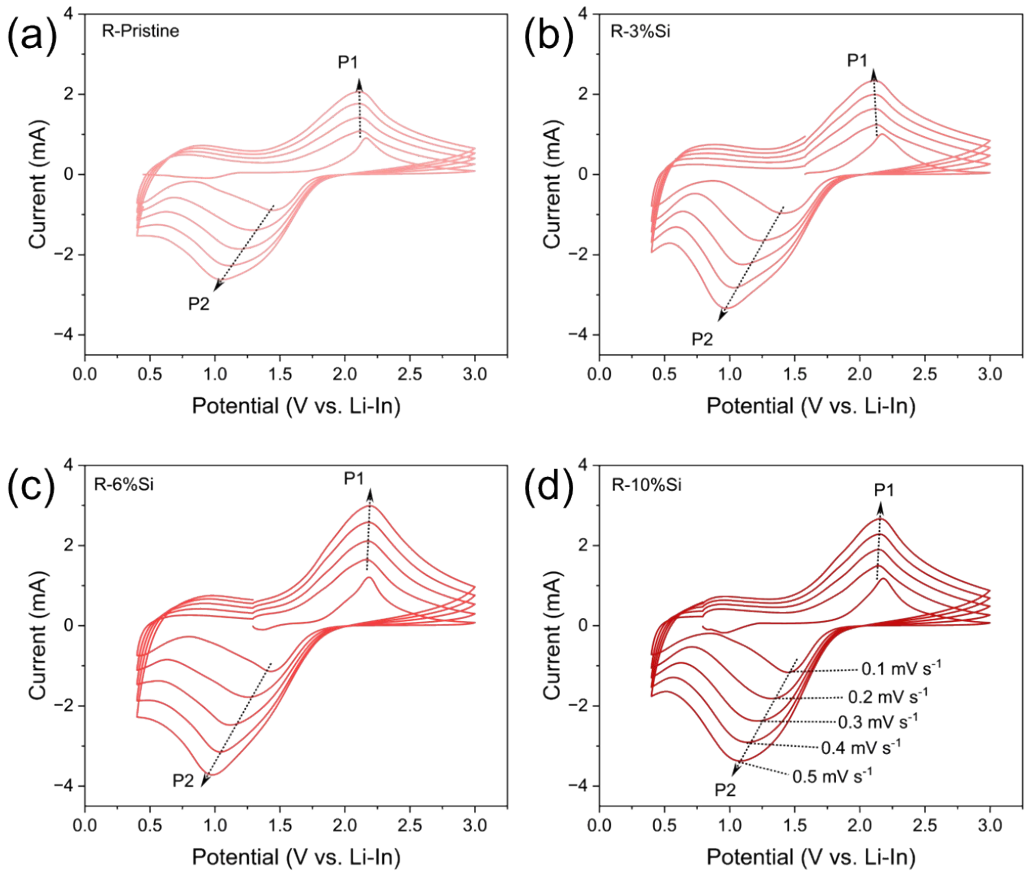

Figure S16 CV curves of (a) R-Pristine, (b) R-3%Si, (c) R-6%Si and (d) R-10%Si at scanning rates of 0.1, 0.2, 0.3, 0.4 and 0.5 mV s^{-1}.

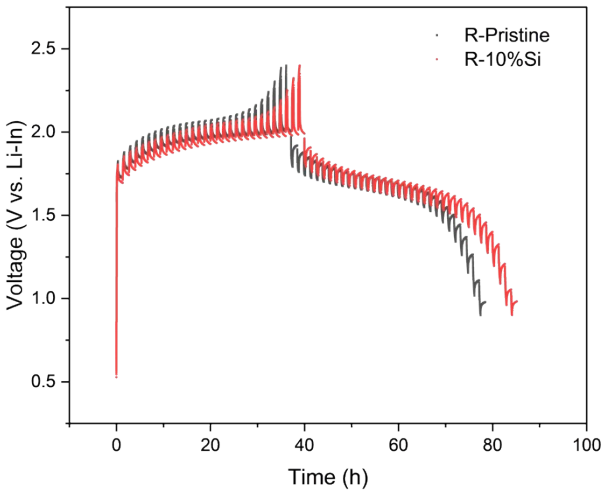

Figure S17 Charge/discharge GITT profiles of R-Pristine and R-10%Si.

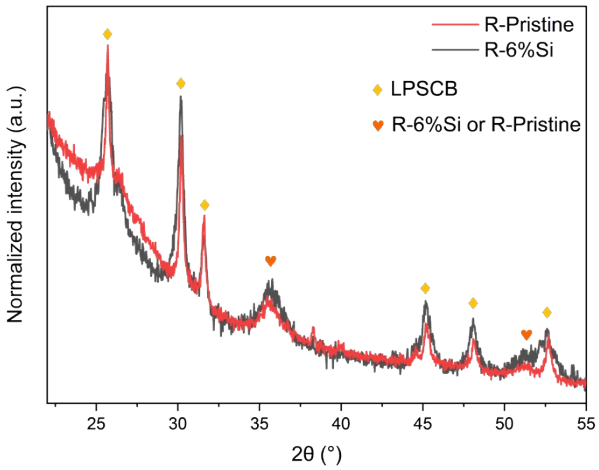

Figure S18 XRD patterns of R-Pristine and R-6%Si composite cathode fully charged (C100%).

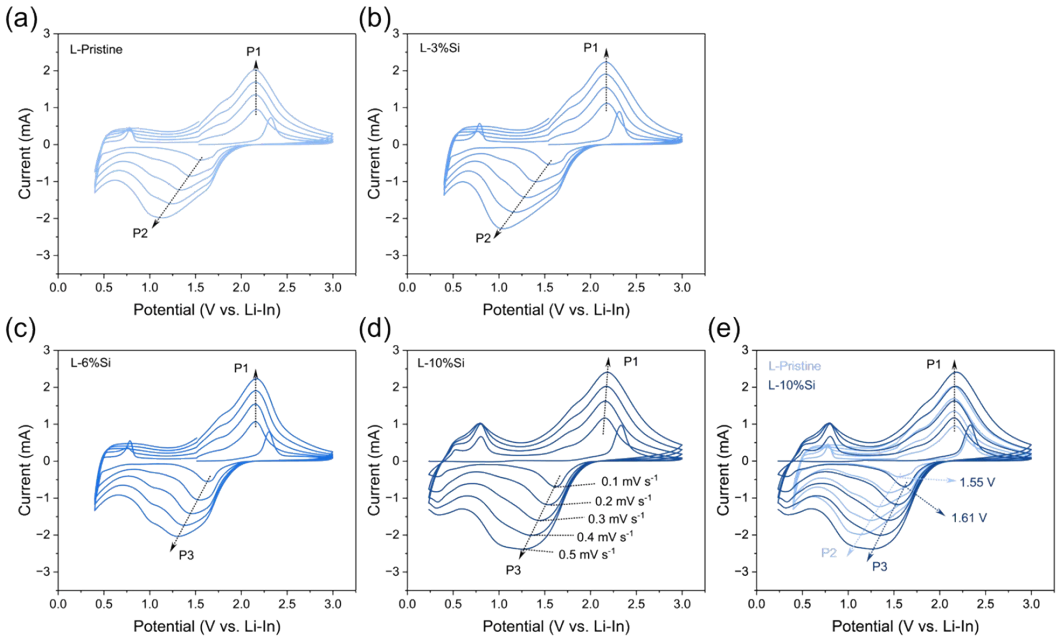

Figure S19 CV curves of (a) L-Pristine, (b) L-3%Si, (c) L-6%Si and (d) L-10%Si at scanning rates of 0.1, 0.2, 0.3, 0.4 and 0.5 mV s^{-1}. (e) Comparison of CV curves for L-Pristine and L-10%Si.

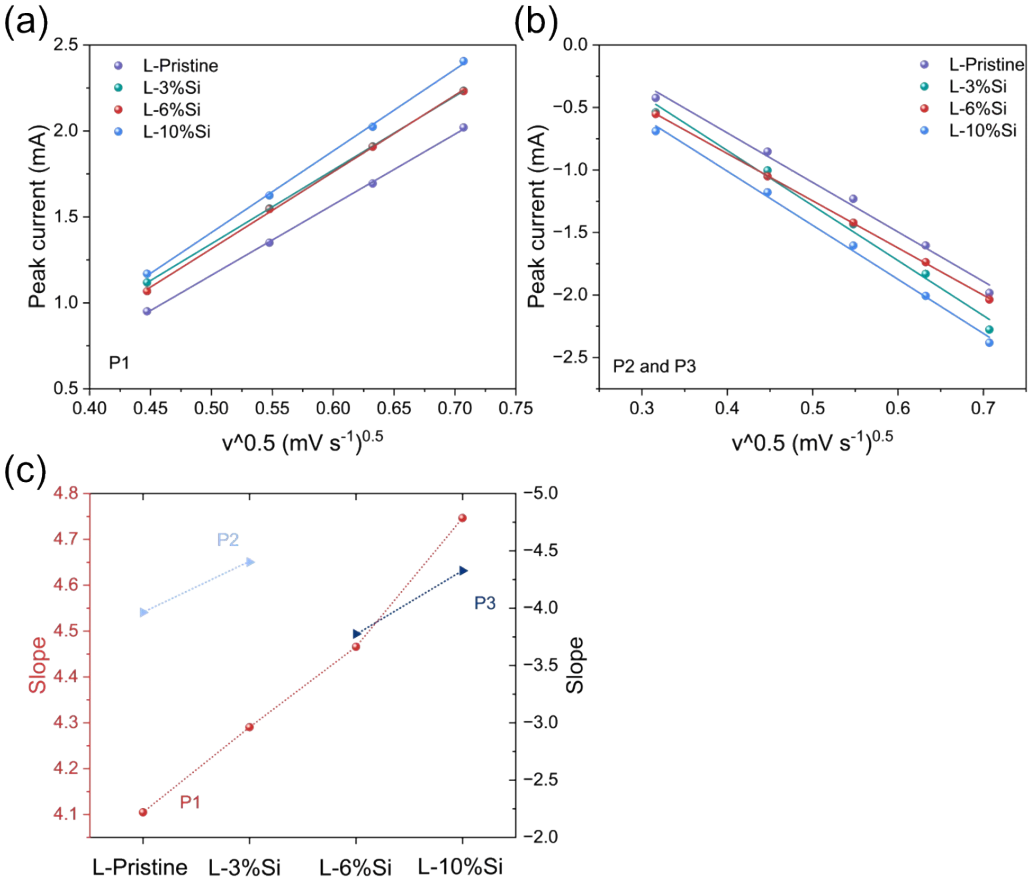

Figure S20 The relationship of (a) oxidation (P1) and (b) reduction (P2 or P3) peak current of different L-$Li_2Ti_{1-x}Si_xS_3$ cathodes versus square root of the scanning rates ($v^{0.5}$). (c) Comparison of slopes of fitted lines in Figure S20 (a) and (b).